2-Butanol Dehydration over Highly Dispersed Molybdenum Oxide/MCM-41 Catalysts

Hyeonhee Choi,[†] Do Heui Kim,[‡] Young-Kwon Park,[§] and Jong-Ki Jeon[†,*]

[†]*Department of Chemical Engineering, Kongju National University, Cheonan 331-717, Korea.*
**E-mail: jkjeon@kongju.ac.kr*
[‡]*School of Chemical and Biological Engineering, Institute of Chemical Processes, Seoul National University, Seoul 151-742, Korea*
[§]*School of Environmental Engineering, University of Seoul, Seoul 130-743, Korea*
Received February 5, 2015, Accepted April 7, 2015, Published online July 27, 2015

Highly dispersed MoO_3 on SiMCM-41 was applied to the dehydration of 2-butanol. MoO_3/MCM-41 catalysts were prepared using a modified atomic layer deposition method. The structural characteristics of MoO_3 supported on SiMCM-41 were examined by inductively coupled plasma spectrometry, nitrogen adsorption, X-ray photoelectron spectroscopy, and X-ray diffraction. The textural characteristics of SiMCM-41 were retained after loading with MoO_3. Ammonia temperature-programmed desorption and Fourier transformation infrared spectroscopy of adsorbed pyridine showed that Lewis acid sites were formed on the MoO_3/MCM-41 catalysts. Among the MoO_3/MCM-41 catalysts, the MoO_3 (16.4 wt %)/MCM-41 catalyst showed the highest catalytic activity for butene synthesis from 2-butanol dehydration due to the largest number of acid sites.

Keywords: Butanol, Dehydration, Butene, Molybdenum oxide, Mesoporous silica

Introduction

Many catalytic reactions are carried out over transition metal oxides.[1–3] Mesoporous materials have been used as a support for metal oxides because of their uniform pore size and large surface area. Highly dispersed transition metal oxides over mesoporous material can be synthesized via modified atomic layer deposition (ALD) technique.[4–8] ALD is a type of the surface sol–gel process that makes thin films of metal oxide grow on a planar surface.[9] The modified ALD technique occurs in four stages, such as the chemisorption of alkoxide, removal of the non-chemisorbed alkoxide precursors by rinsing with a solvent, hydrolysis of the chemisorbed alkoxide, and drying.[9]

C_4H_8 is generally produced by the naphtha cracking process in the petrochemical industry. Recently, because the naphtha cracking process has been replaced with a C_2H_6 cracker, there has been an overall shortage of butenes. In addition, an ethane cracking process based on the process in the shale gas industry has recently been established. Because the C_2H_6 cracking reaction generates a large amount of C_2H_4 with no C_4H_8, there will be mismatch between the supply and demand in the C_4H_8 market. To meet the demand of C_4H_8, it is essential to develop innovative chemical technologies and introduce new raw materials for the production of butenes. Bio-butanol converted from cellulose has attracted considerable attention as a biofuel and has been recognized as an alternative to bio-ethanol. Recently, many technologies for producing fuel and chemical products from bio-butanol have been developed by several researchers.[10,11]

Previous studies demonstrated that aluminosilicates with an ordered structure can be used for butanol dehydration.[8] In addition, WO_3 supported on mesoporous silica could be used to produce butenes through butanol dehydration.[12] This study focused on highly dispersed MoO_3 on SiMCM-41 prepared using a modified ALD method. The Brunauer-Emmett-Teller (BET) method, inductively coupled plasma spectrometry (ICP), X-ray photoelectron spectroscopy (XPS), X-ray diffraction (XRD), Fourier transformation infrared spectroscopy (FTIR) of adsorbed pyridine, and NH_3 temperature-programmed desorption were used to examine the physicochemical characteristics of the supported MoO_3 catalysts. The catalytic performance in butanol dehydration was evaluated in continuous gas flow with a packed bed reactor.

Experimental

SiMCM-41 was synthesized using the method described elsewhere.[12–15] Molybdenum oxide was grafted over SiMCM-41 via the modified ALD method.[6,12] SiMCM-41 powder was suspended in toluene and heated under reflux for 4 h in bubbling N_2. $MoOCl_4$ was also suspended in toluene and heated under reflux for 8 h under N_2 atmosphere. The solution containing SiMCM-41 was mixed with a $MoOCl_4$ solution and heated under reflux for 24 h under a nitrogen atmosphere. The mixed solution was washed with toluene, filtered, dried at 373 K in an oven, and finally calcined at 773 K in a furnace. The amount of $MoOCl_4$ in the precursor solution was varied to obtain a range of molybdenum oxide loadings (4.4, 10.5, 12.5, and 16.4 wt %) on MCM-41 (MoO_3/MCM-41). A MoO_3/MCM-41 sample containing more than 16.4 wt % MoO_3 loading could not be obtained even when an excess of $MoOCl_4$ solution was used.

The N_2 adsorption isotherms of the catalysts were obtained using a Bel Sorp-mini (Bel Japan Inc., Osaka, Japan) at 77 K. The surface area was measured using the BET equation. The pore volume and pore size were obtained according to the t-plot and the Barrett-Joyner-Halenda (BJH) method, respectively. The crystalline structure of the catalysts was examined by XRD. ICP (Flame Modula S, Spectro, Kleve, Germany) was used to determine the amount of molybdenum in the catalyst. XPS (MultiLab ESCA 2000, Thermo Fisher Scientific Inc., Waltham, MA, USA) was conducted using MgKα radiation (300 W) to determine the oxidation state of molybdenum oxide on SiMCM-41.

The nature of the acid sites over the MoO_3/MCM-41 catalysts was investigated using pyridine as a probe molecule.[12] Fourier transform infrared (FTIR) spectroscopy of the adsorbed pyridine (Pyridine-IR) over the catalysts was performed in a transmission infrared cell. The strength and amount of the acid sites over the catalysts were measured according to the temperature-programmed desorption of ammonia (ammonia-TPD) using a BEL-CAT-B (Bel Japan Inc., Osaka, Japan).[8,16]

The dehydration reaction of 2-butanol was carried out over 0.02 g of MoO_3/MCM-41 catalysts in a packed bed reactor. After heating the catalyst bed to a certain temperature under a N_2 flow (400 cc/min), 2-butanol was provided with a flow in a range of 2–16 cc/h using a syringe pump. The N_2 flow was controlled using a mass flow controller. After evaporating 2-butanol through a pre-heater, 2-butanol was injected into the reactor in the gas phase. The temperature of the catalyst bed was adjusted with a tubular electric furnace equipped with a temperature controller. The gaseous products were analyzed by gas chromatography (YL 6100 GC, YL Instrument, Seoul, Korea) equipped with a flame ionization detector and an aluminum oxide capillary column.

Results and Discussion

Figure 1 presents the N_2 adsorption-desorption isotherms of SiMCM-41 and MoO_3/MCM-41. The N_2 adsorption-desorption isotherms show that all the catalysts exhibited hysteresis, a characteristic of mesoporous materials.[17] All catalysts exhibited typical type IV isotherm curves with a hysteresis loop (H1 type) at P/P_0 between 0.3 and 0.4. As the amount of molybdenum oxide loading increased, the shape of the hysteresis loop was similar despite the reduced amount of N_2 adsorbed. This suggests that the shape of pores may be almost uniform through the molybdenum oxide deposition process.

Table 1 lists the BET surface area, pore size, and total pore volume of the catalysts. The BET surface area and total pore volume of SiMCM-41 were 1059 m^2/g and 0.97 cm^3/g, respectively. With increased molybdenum oxide loading up to 16.4 wt %, the BET surface area and the total pore volume decreased to 885 m^2/g and 0.74 cm^3/g, respectively. The pore size of SiMCM-41 was 3.0 nm, but it decreased slightly with increasing molybdenum oxide loading, which can be attributed to the reduction of the available void volume.

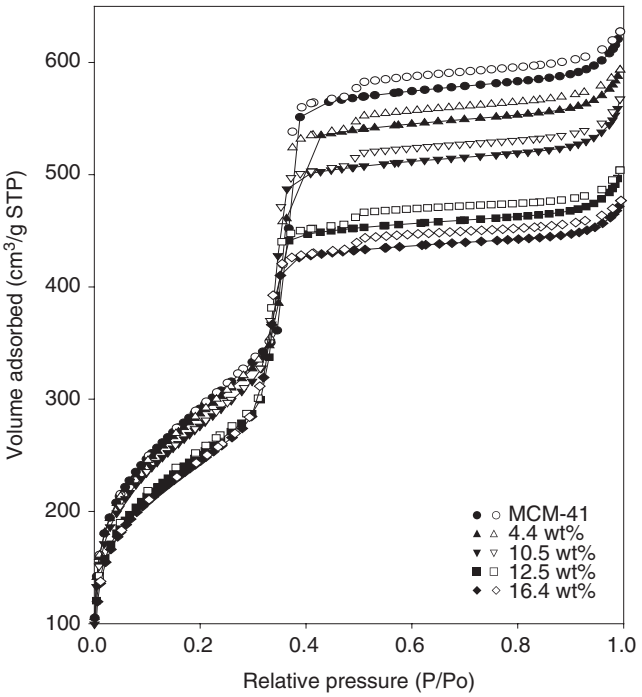

Figure 1. N_2 adsorption-desorption isotherms of the MoO_3/MCM-41 catalysts (Filled symbol: adsorption, unfilled symbol: desorption).

Table 1. BET surface area, pore volume, and pore size of the MoO_3/MCM-41 catalysts.

MoO_3 loading (wt %)	S_{BET} (m^2/g)	V_P[a] (cm^3/g)	Pore size[b] (nm)
0	1059	0.97	3.0
4.4	1025	0.88	3.0
10.5	1001	0.81	2.9
12.5	907	0.78	2.9
16.4	885	0.74	2.8

[a] Pore volume measured at $P/P_0 = 0.99$.
[b] Average diameter of mesopores calculated by BJH method.

Figure 2 shows the XRD patterns for the SiMCM-41 and MoO_3/MCM-41 catalysts. The small-angle XRD patterns of the catalysts in Figure 2(a) show one intense peak and two weak peaks that can be assigned to the (100), (110), and (200) reflections and are characteristic of a 2-D hexagonal mesoporous structure.[18] These peaks show that the skeletal structure of SiMCM-41 is quite uniform. The ordered hexagonal structures of the MoO_3/MCM-41 catalysts, even at high molybdenum oxide loadings, were confirmed by the low-angle XRD results. All the samples showed similar characteristics, suggesting that the mesoporous structure of the SiMCM-41 can be retained after loading with molybdenum oxide. More importantly, the XRD peaks arising from the molybdenum oxides were not detected at higher angles for any of the catalysts (Figure 2(b)). These results clearly mean that the molybdenum oxide phases are highly dispersed over

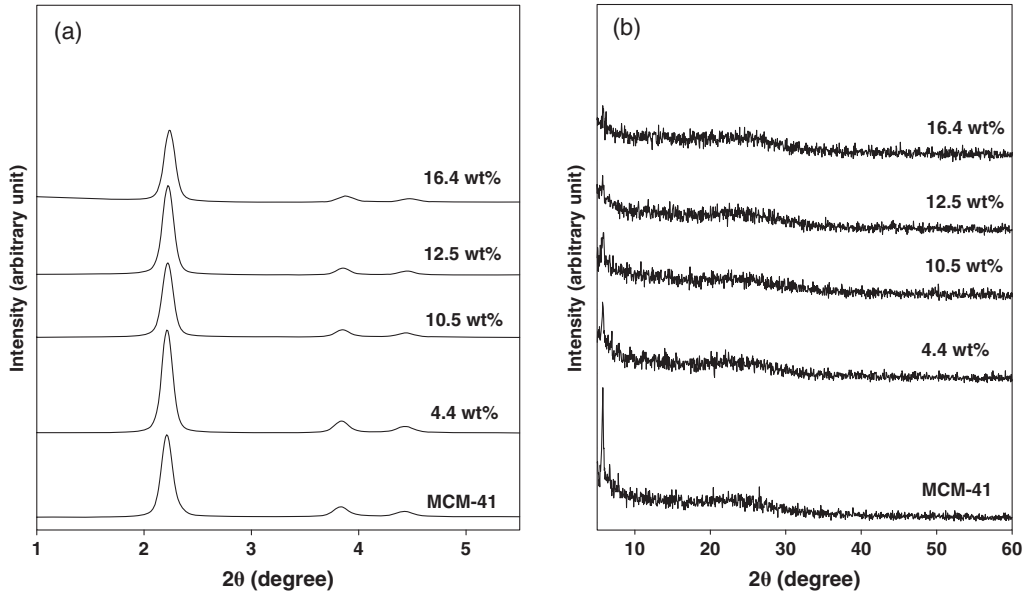

Figure 2. XRD patterns of the MoO_3/MCM-41 catalysts (a) low-angle XRD, (b) high-angle XRD.

the MCM-41 surface, even with a high molybdenum oxide loading.

Figure 3 shows the molybdenum 3d XP spectra of the catalysts. The Mo 3d spectra had two peaks ($3d_{5/2}$ and $3d_{3/2}$), which were separated by 3.1 eV. All four samples contained Mo^{6+} (e.g., MoO_3) because their main Mo $3d_{5/2}$ peaks were located at 232.6 eV.[19] As marked in Figure 3, no oxidation state other than MoO_3 was observed in these samples, suggesting that the modified ALD method can produce the same MoO_3 species on MCM-41 within this molybdenum oxide loading range. Moreover, the surface coverage of MoO_3 on MCM-41 increased in proportion to the Mo loading, as evidenced by the increase in the area of the Mo 3d peak. Cl 2p peaks were not detected in any of the samples, indicating complete calcination (not shown).

Figure 4 shows the effect of the molybdenum oxide loading over SiMCM-41 on the ammonia-TPD profiles. It was difficult to find a peak in the ammonia-TPD curve of SiMCM-41, which means that there are few acid sites over the SiMCM-41 surface. The MoO_3/MCM-41 catalysts exposed weak acid sites at 170 °C, whereas strong acid sites could not be detected, indicating that only weak acid sites were generated upon the molybdenum oxide loading. As summarized in Table 2, the total amount of acid sites was found to increase with increasing molybdenum oxide loading.

Figure 5 shows the FTIR spectra of adsorbed pyridine over MoO_3(12.5 wt %)/MCM-41 followed by desorption at a temperature range of 25–300 °C under 10^{-3} torr. At lower temperatures (<100 °C), two distinct peaks were detected at 1593 and 1445 cm^{-1}. An increase in desorption temperature appeared to decrease the intensity of the two peaks at 1593 and 1445 cm^{-1} more considerably than that of the three peaks at 1611, 1575, and 1454 cm^{-1}. Finally, the peaks at 1611 and 1454 cm^{-1} were obvious after desorption at 300 °C. The two

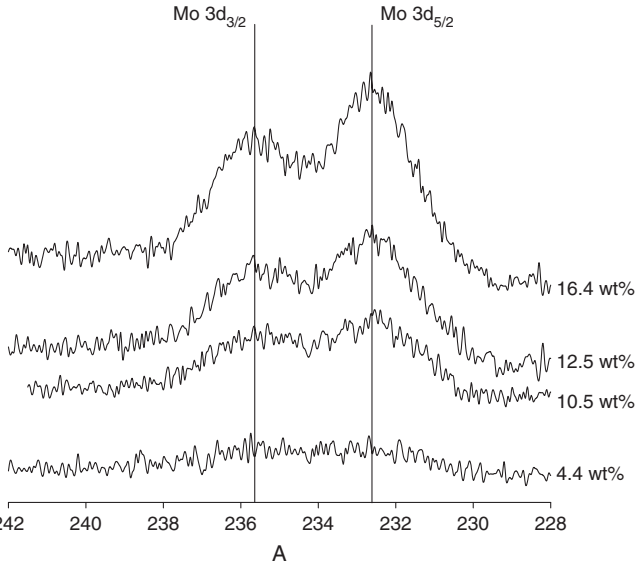

Figure 3. Mo 3d photoelectron spectra of the molybdenum oxide/MCM-41 catalysts.

peaks at 1611 and 1454 cm^{-1} indicate the occurrence of acid sites with higher strength than the two peaks at 1593 and 1445 cm^{-1}. These tendencies are well consistent with those described in the literature.[20–24] The peaks at 1611, 1575, and 1454 cm^{-1} could be indexed to Lewis acid sites. The peaks at 1593 and 1445 cm^{-1} were reported to be peaks that could be generated by hydrogen-bonded pyridine with Si-OH group.[20–24]

The FTIR spectra of pyridine adsorbed over the catalysts at 150 °C are shown in Figure 6. The SiMCM-41 catalyst showed two peaks at 1445 and 1593 cm^{-1}, which were assigned to the peaks produced by hydrogen-bonded pyridine (H).[13] This indicates that the SiMCM-41 catalyst has neither

Brønsted acid sites (B) nor Lewis acid sites (L). In addition to the H sites, Lewis acid sites were generated over the MoO_3/MCM-41 catalysts, which resulted from the formation of MoO_3-induced acid sites. The relative intensity of the peak at 1611 cm^{-1} to that at 1593 cm^{-1} increased with increasing MoO_3 loading. This suggests that the amount of Lewis acid sites increases with increasing MoO_3 loading over MCM-41. Both the ammonia-TPD and infrared spectra of the adsorbed pyridine results mean that weak acid sites, primarily Lewis acid sites, were generated over the MoO_3/MCM-41 catalysts.

The catalytic activity for the dehydration of 2-butanol over the six catalysts was investigated in a packed bed reactor. First of all, it was confirmed that 2-butanol barely converted without a catalyst at a temperature range of 200 to 250 °C, 1 atm reaction pressure, and a weight hour space velocity (WHSV, based on flow rate of 2-butanol) of 80 h^{-1}. Figure 7 presents the conversion of 2-butanol and selectivity to butenes. As expected, 2-butanol conversion was very low over pure MoO_3. While SiMCM-41 with no molybdenum oxide content recorded less than 2.6% 2-butanol conversion at 200 °C and a WHSV of 80 h^{-1}, the conversion of 2-butanol increased drastically with increasing molybdenum oxide loading. Eventually, the catalyst with a 16.4 wt % molybdenum oxide loading showed approximately 26.3% conversion of

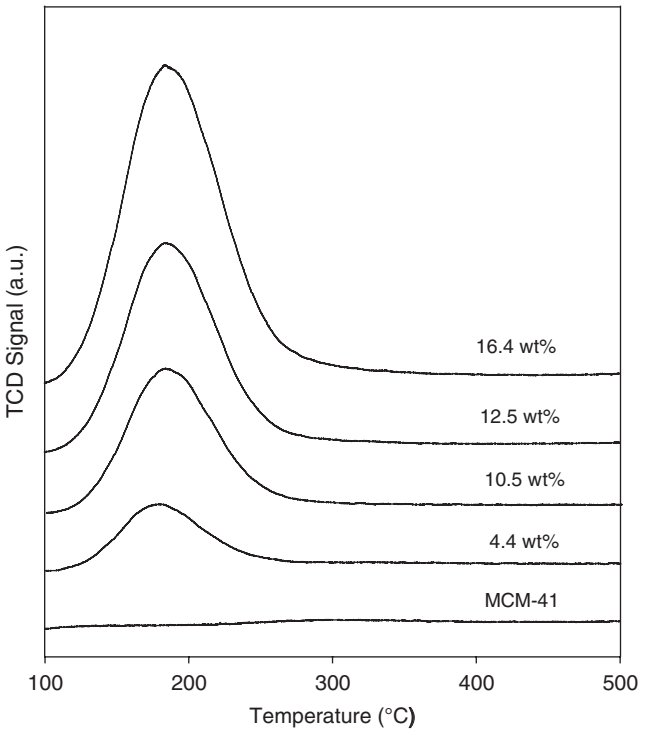

Figure 4. Ammonia-TPD of MoO_3/MCM-41 catalysts.

Table 2. Acidity of various catalysts by ammonia-TPD.

MoO_3 loading (wt %)	Total acidity (mmol/g)
0	0.2
4.4	0.9
10.5	0.8
12.5	1.0
16.4	1.5

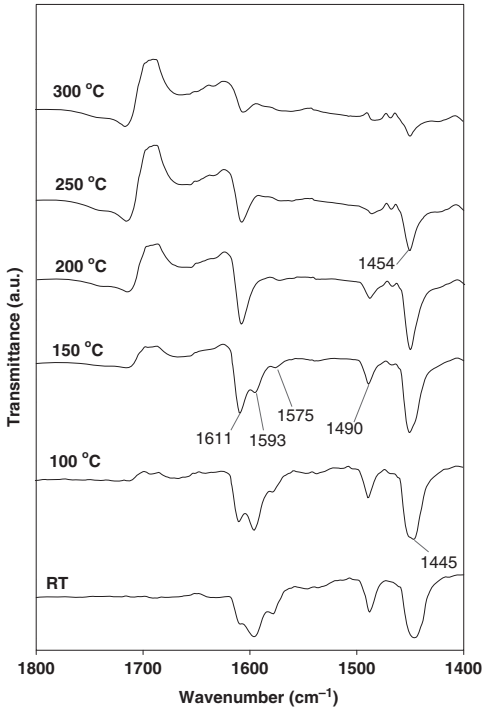

Figure 5. Infrared spectra of adsorbed pyridine over MoO_3 (12.5 wt %)/MCM-41 under 10^{-3} torr.

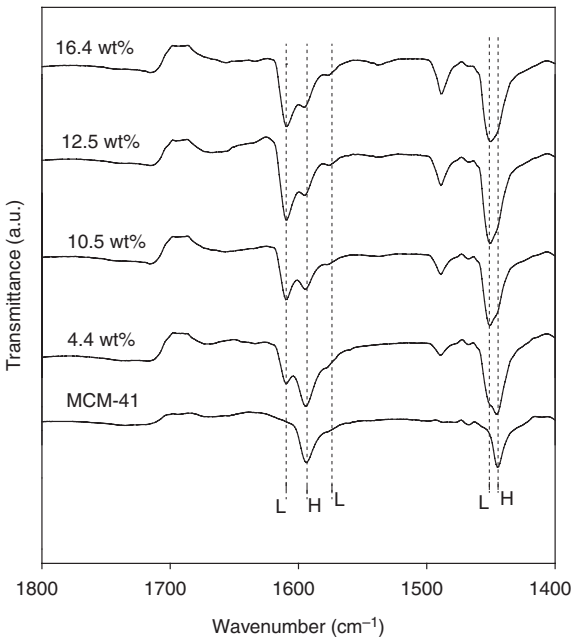

Figure 6. Infrared spectra of adsorbed pyridine over the MoO_3/MCM-41 catalysts at 150 °C under 10^{-3} torr.

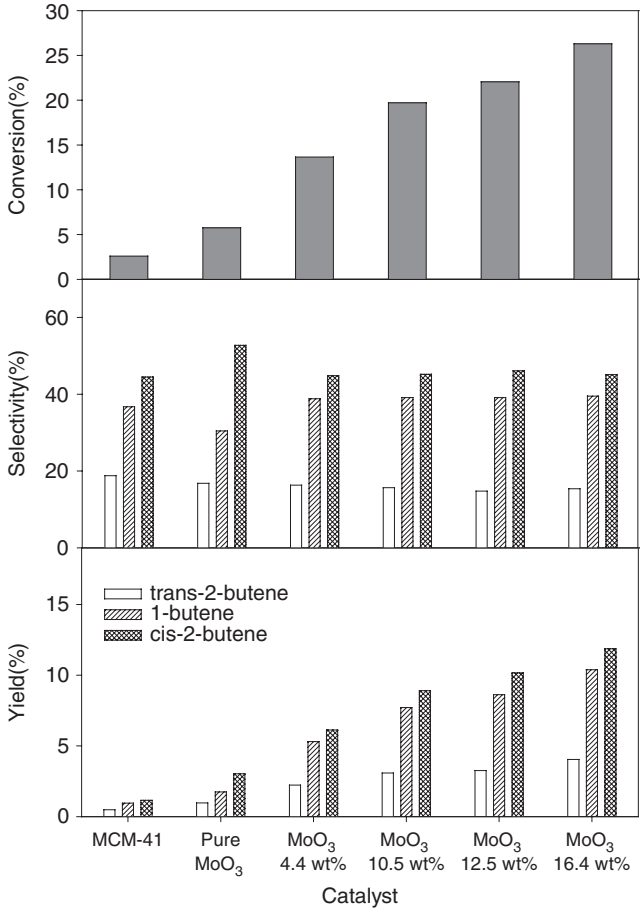

Figure 7. Conversion, selectivity, and yield of 2-butanol dehydration over various catalysts (Reaction conditions: 200 °C, 1 atm, WHSV 80 h^{-1}, time-on-stream 2 h).

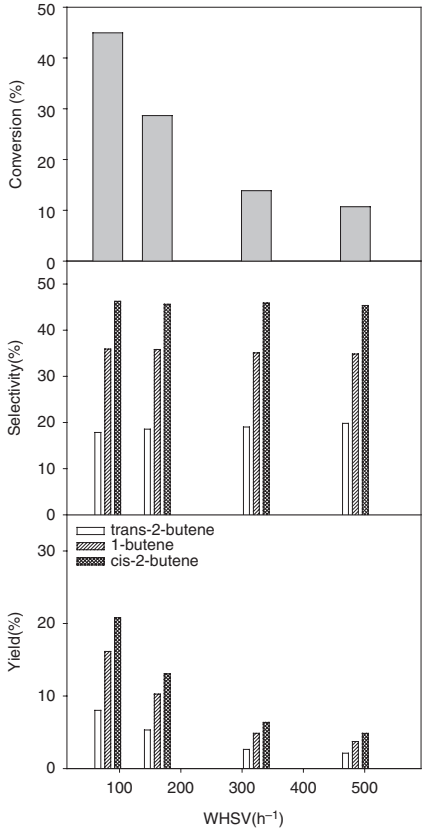

Figure 8. Effect of WHSV on conversion and product distribution over MoO_3 (12.5 wt %)/MCM-41 catalyst (Reaction condition: 250 °C, 1 atm, time-on-stream 2 h).

2-butanol. As shown in Figure 4, the ammonia-TPD confirmed that the four catalysts had similar acid site strengths. In addition, the acid sites over the MoO_3/MCM-41 catalysts consisted of Lewis acid sites and H-bonded weak acid sites. Therefore, the highest activity of the MoO_3/MCM-41 catalyst with the 16.4 wt % molybdenum oxide loading can be attributed to the large number of acid sites among the five catalysts. The selectivity to cis-2-butene was highest over the MCM-41 and molybdenum oxide-introduced catalysts. The product distribution in 2-butanol dehydration, however, was not altered considerably with increasing molybdenum oxide loading.

The effect of the space velocity on the catalytic performance in 2-butanol dehydration was also investigated over the MoO_3 (12.5 wt %)/MCM-41 catalyst (Figure 8). When the space velocity was changed from 80 h^{-1} to 480 h^{-1}, a significant decrease in the conversion of 2-butanol was observed, but product distribution was not changed. Consequently, although SiMCM-41 is inactive for the dehydration of 2-butanol, highly dispersed molybdenum oxide on SiMCM-41 synthesized using a modified ALD method can serve as a catalyst for butene synthesis from 2-butanol.

Conclusion

MoO_3/MCM-41 catalysts were prepared by modified ALD technique. The textural characteristics of the molybdenum oxide supported on SiMCM-41 were the same as those on the bare catalyst. Ammonia-TPD and FTIR spectroscopy of adsorbed pyridine indicated the formation of weak acid sites, primarily Lewis acid sites, on the MoO_3/MCM-41 catalysts. The MoO_3(16.4 wt %)/MCM-41 catalyst showed the highest catalytic activity for 2-butanol dehydration due to the largest number of acid sites among the MoO_3/MCM-41 catalysts.

Acknowledgments. This research was supported by the Basic Science Research Program through the National Research Foundation of Korea (NRF) funded by the Ministry of Education, Science and Technology (grant number 2010-0023600).

References

1. J. H. Kwak, J. E. Herrera, J. Z. Hu, Y. Wang, C. H. F. Peden, *Appl. Catal. A* **2006**, *300*, 109.
2. A. F. Perez-Cadenas, C. Moreno-Castilla, F. J. Maldonado-Hodar, J. L. G. Fierro, *J. Catal.* **2003**, *217*, 30.
3. J. C. Vartuli, J. G. Santiesteban, P. Traverso, N. C. Martinez, C. D. Chang, S. A. Stevenson, *J. Catal.* **1999**, *187*, 131.

4. Y. Wang, K. Y. Lee, S. Choi, J. Liu, L. Q. Wang, C. H. F. Peden, *Green Chem.* **2007**, *9*, 540.
5. J. Macht, C. D. Baertsch, M. May-Lozano, S. L. Soled, Y. Wang, E. Iglesia, *J. Catal.* **2004**, *227*, 479.
6. J. E. Herrera, J. H. Kwak, J. Hu, Y. Wang, C. H. F. Peden, J. H. Macht, E. Iglesia, *J. Catal.* **2006**, *239*, 200.
7. J. E. Herrera, J. H. Kwak, J. Hu, Y. Wang, C. H. F. Peden, *Top. Catal.* **2006**, *39*, 245.
8. S. Jeong, H. Kim, J. H. Bae, D. H. Kim, C. H. F. Peden, Y. K. Park, J. K. Jeon, *Catal. Today* **2012**, *185*, 191.
9. I. Ichinose, H. Senzu, T. Kunitake, *Chem. Lett.* **1996**, *25*, 831.
10. Z. Hasan, J. W. Jun, S. H. Jhung, *Chem. Eng. J.* **2015**, *278*, 265.
11. J. W. Jun, J. Jeon, C. U. Kim, K. E. Jeong, S. Y. Jeong, S. H. Jhung, *J. Nanosci. Nanotechnol.* **2013**, *13*, 2782.
12. H. J. Kim, S. Y. Jeong, D. H. Kim, Y. K. Park, J. K. Jeon, *J. Nanosci. Nanotechnol.* **2012**, *12*, 6074.
13. J. K. Jeon, H. Lee, J. H. Yim, Y. S. Kim, S. J. Lee, Y. K. Park, J. K. Shon, J. M. Kim, *Catal. Lett.* **2007**, *19*, 179.
14. S. Yun, M. Seong, Y. K. Park, S. Y. Jeong, J. Han, J. K. Jeon, *J. Nanosci. Nanotechnol.* **2015**, *15*, 647.
15. R. Ryoo, J. M. Kim, *J. Chem. Soc. Chem. Commun.* **1995**, 711.
16. S. Y. Hosseini, M. R. K. Nikou, *J. Ind. Eng. Chem.* **2014**, *20*, 4421.
17. S. A. Bagshaw, N. I. Baxter, D. R. M. Brew, C. F. Hosie, N. Yuntong, S. Jaenicke, C. G. Khuan, *J. Mater. Chem.* **2006**, *16*, 2235.
18. H. I. Lee, H. J. Park, Y. K. Park, J. Y. Hur, J. K. Jeon, J. M. Kim, *Catal. Today* **2008**, *132*, 68.
19. J. F. Moulder, J. Chastain, *Handbook of X-Ray Photoelectron Spectroscopy: A Reference Book of Standard Spectra for Identification and Interpretation of XPS Data*, Eden Prairie, MN, Physical Electronics Division, Perkin-Elmer, **1992**.
20. B. Chakraborty, B. Viswanathan, *Catal. Today* **1999**, *49*, 253.
21. G. T. Palomino, J. J. C. Pascual, M. R. Delgado, J. B. Parra, C. O. Arean, *Mater. Chem. Phys.* **2004**, *85*, 145.
22. M. I. Zaki, M. A. Hasan, F. A. Al-Sagheer, L. Pasupulety, *Colloids Surf. A* **2001**, *190*, 261.
23. J. K. Jeon, D. H. Kim, Y. K. Park, *Bull. Korean Chem. Soc.* **2014**, *35*, 2669.
24. F. Guo, S. Guo, X. X. Wei, X. Wang, H. Xiang, Z. Qiu, L. Zhao, *Korean J. Chem. Eng.* **2014**, *31*, 1973.

